Vol. 12, No. 4, 2021
ISSN 2233-4203/ e-ISSN 2093-8950
ARTICLE www.msletters.org | Mass Spectrometry Letters

Integrated Thermochemical Approach to Collision-Induced Dissociation Process of Peptides

Seung Koo Shin* and Hye-Joo Yoon

Bionanotechnology Center, Department of Chemistry, Pohang University of Science and Technology, Pohang, Kyungbuk, 37673, Korea

Received November 30, 2021; Revised December 08, 2021; Accepted December 08, 2021
First published on the web December 31, 2021; DOI: 10.5478/MSL.2021.12.4.131

Abstract : Collision-induced dissociation of peptides involves a series of proton-transfer reactions in the activated peptide. To describe the kinetics of energy-variable dissociation, we considered the heat capacity of the peptide and the Marcus-theory-type proton-transfer rate. The peptide ion was activated to the high internal energy states by collision with a target gas in the collision cell. The mobile proton in the activated peptide then migrated from the most stable site to the amide oxygen and subsequently to the amide nitrogen (N-protonated) of the peptide bond to be broken. The N-protonated intermediate proceeded to the product-like complex that dissociated to products. Previous studies have suggested that the proton-transfer equilibria in the activated peptide affect the dissociation kinetics. To take the extent of collisional activation into account, we assumed a soft-sphere collision model, where the relative collision energy was fully available to the internal excitation of a collision complex. In addition, we employed a Marcus-theory-type rate equation to account for the proton-transfer equilibria. Herein, we present results from the integrated thermochemical approach using a tryptic peptide of ubiquitin.

Keywords : energy-variable CID, thermochemical approach, soft-sphere collision, Marcus theory of proton transfer

Introduction

Collision-induced dissociation (CID) is a powerful technique used in mass spectrometry (MS) for the identification of peptides and the quantification of proteins.[1] Peptide ions are generated in the gas phase by soft ionization techniques like electrospray ionization (ESI) and matrix-assisted laser desorption/ionization (MALDI), and they carry protons embedded in the most stable sites. For tandem MS analysis, the peptide ion of interest is mass-selected and accelerated into a collision cell to induce dissociation. The accelerated ion collides with the target gas, such as argon, nitrogen and xenon, which leads to an increase in internal energy of the peptide ion. As a result, the activated peptide ion fragments into various sequence-specific and -nonspecific products. For a given amino acid sequence and a charge state, the fragmentation pattern changes with the collision energy, the transit time in a collision cell and the instrument response function.

In this work, we are interested in the hydrogen-bonding environment in the protonated peptide rather than the fragmentation pattern. At the low collision energy, the activated peptide ion usually undergoes backbone dissociation to yield sequence ions like b- and y-type products containing the N- and C-termini, respectively. A current consensus is that the backbone dissociation involves a series of intramolecular proton-transfer reactions from the most stable site to the amide oxygen (O-protonated) and subsequently to the amide nitrogen (N-protonated) of the peptide bond to be broken, which is termed the 'mobile proton' model.[2–7] Then, the N-protonated intermediate undergoes a dissociative intramolecular rearrangement to yield the product-like complex that fragments into the b and y product ions.[3–5] This mobile proton model implies that the hydrogen-bonding environment in the intact peptide ion acts as a cage for the intramolecular proton transfer reactions.[6] When the proton migrates between the most stable site and the backbone amide within the cage, the promotion energy is required to reorganize the nuclei of the peptide ion to accommodate the proton migration, thereby affecting the dissociation kinetics.

Open Access
*Reprint requests to Seung Koo Shin
https://orcid.org/0000-0002-8294-2119
E-mail: skshin@postech.ac.kr

This article is part of the special issue in honor of Professor Seung Koo Shin.

Thus, the overall reaction can be written as the following scheme:

$$R + M \rightarrow R^* \rightleftharpoons I_O \rightleftharpoons I_N \rightarrow b \cdot y \rightarrow \text{products}, \quad (1)$$

where R is the intact peptide ion carrying a proton at the most stable site, M is the target gas, R^* is the activated peptide ion, I_O is the O-protonated intermediate, I_N is the N-protonated intermediate, b·y is the dissociative product-like complex, and products are b/y ions and their neutral counterparts.

Methods

Marcus theory of proton transfer

We assumed that the intact peptide ion R was stabilized by forming a hydrogen-bond network between the protonated site and the carbonyl oxygen of backbone amides. Typical hydrogen bonds involve the donor–hydrogen–acceptor bond angle of less than 30° and the donor-to-acceptor bond distance of shorter than 3.0 Å.[8] Within the hydrogen-bond network, R^*, I_O and I_N can donate or accept the proton. We adopted a Marcus-theory-type rate equation to describe the intramolecular proton transfer within the hydrogen-bond network.[9,10] The consecutive proton-transfer equilibria from R^* to I_O and subsequently to I_N can be combined into a single process from R^* to I_N, as shown in Figure 1.

If $\Delta G^\dagger$ is given by the point of intersection A between the two parabolic curves for donor R and acceptor I_N in Figure 1, then $\Delta G^\dagger$ can be written in terms of E_m and ΔG^0, as given in eq 2:[11]

$$\Delta G^\dagger = \frac{(E_m + \Delta G^0)^2}{4E_m}. \quad (2)$$

E_m represents the vertical energy required to reorganize the nuclei of the acceptor into the donor configuration B in the absence of the proton back transfer. The rate constant for the proton-transfer reaction k_{PT} is thus:[11]

$$k_{PT} = \frac{k_B T}{h}\exp\left(-\frac{\Delta G^\dagger}{RT}\right) = \frac{k_B T}{h}\exp\left(-\frac{(E_m + \Delta G^0)^2}{4E_m RT}\right), \quad (3)$$

where k_B is the Boltzmann constant, T is the temperature of the activated peptide ion, h is the Planck constant, and R is the gas constant.

For I_N, however, the hydrogen-bond network between the N-protonated amide and the surrounding nuclei is weakly bound in comparison with those in the intact peptide ion. Once the hydrogen-bond network is disintegrated, I_N proceeds to the dissociative rearrangement reaction that involves a nucleophilic attack of the carbonyl oxygen at the adjacent N-terminal side on the trivalent carbon of the N-protonated intermediate to form a product-like b·y complex between the protonated oxazolone derivative and the neutral C-terminal fragment. This reaction is considered to be irreversible in the time scale of CID experiments because the complex b·y dissociates fast to products and the backward reaction is entropically hindered. The final dissociation step consists of the two competing reactions, one yielding a b ion with a neutral C-terminal fragment and the other providing a complementary y ion with a neutral oxazolone derivative.[4] The product branching ratio is presumably determined by the difference in free energy between the two product channels.[7] Consequently, the rate of product appearance is proportional to the concentration of the N-protonated intermediate.

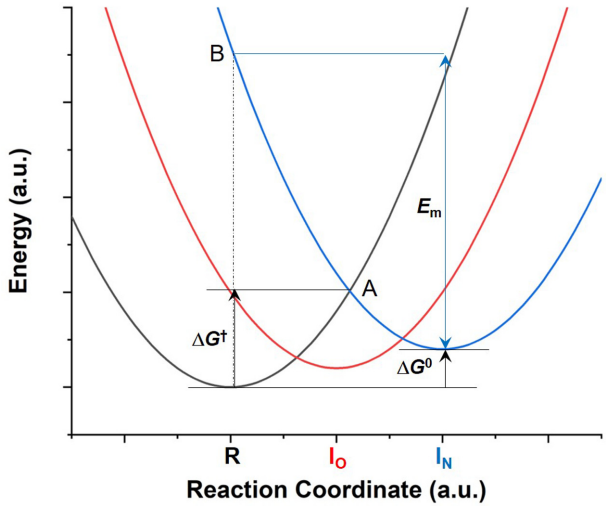

Figure 1. Energy dependence as a function of reaction coordinate for the proton on donor R or acceptor I_N via intermediate I_O. ΔG^0 is the free energy of the proton-transfer reaction from R to I_N, E_m is the Marcus reorganization energy and $\Delta G^\dagger$ is the free energy of the transition state relative to R.

Overall dissociation kinetics

Taken all together, we can further simplify the overall reaction as the following scheme:

$$R + M \xrightarrow{k_1} R^* \xrightarrow{k_{PT}} I_N \xrightarrow{k_2} \text{products}. \quad (4)$$

The first step results in the collisional activation of the intact peptide ion, the second step involves the proton transfer from the activated peptide ion to the N-protonated intermediate through the hydrogen-bond network, and the last step is the dissociation to products.

The rate constant k_1 denotes the rate of collision between the peptide ion and the target gas in the collision cell, which can be expressed in terms of the collision cross section σ, the velocity of the accelerated peptide ion v, and

the pressure of the target gas [M], as given in eq 5:

$$k_1 = \sigma v[\mathrm{M}]\,. \tag{5}$$

The rate constant for proton transfer k_{PT} is described earlier in eq 3. If the rate constant k_2 is much greater than k_{PT}, then the steady-state concentration of I_N is very small and the sum of $[I_N]$ and [products] represents the net concentration of I_N resulting from the proton-transfer reaction. The time-dependent concentrations of R, R^* and I_N plus products are thus:

$$\begin{aligned}
&[\mathrm{R}] = [\mathrm{R}]_0 \exp(-k_1 t),\\
&[\mathrm{R}^*] = [\mathrm{R}]_0 \frac{k_1}{k_{\mathrm{PT}} - k_1}\left[\exp(-k_1 t) - \exp(-k_{\mathrm{PT}} t)\right],\\
&[\mathrm{I_N}] + [\mathrm{products}] = [\mathrm{R}]_0 - [\mathrm{R}^*] - [\mathrm{R}]\\
&= [\mathrm{R}]_0 \left\{1 - \frac{k_1}{k_{\mathrm{PT}} - k_1}\left[\exp(-k_1 t) - \exp(-k_{\mathrm{PT}} t)\right] - \exp(-k_1 t)\right\},
\end{aligned} \tag{6}$$

where $[R]_0$ is the initial concentration of the intact peptide ion. The sum of $[R]/[R]_0$ and $[R^*]/[R]_0$ represents the fraction of the peptide ion survived from the reaction, as given in eq 7:

$$\frac{[\mathrm{R}] + [\mathrm{R}^*]}{[\mathrm{R}]_0} = \frac{k_{\mathrm{PT}} \exp(-k_1 t) - k_1 \exp(-k_{\mathrm{PT}} t)}{k_{\mathrm{PT}} - k_1}\,. \tag{7}$$

We used eq 7 to calculate the survival fraction of a tryptic peptide LIFAGK of ubiquitin as a function of collision energy.

Soft-sphere model for collision

Details of energy-variable CID experiments have been published elsewhere.[12] In brief, experiments were carried out using a hybrid triple quadruple time-of-flight (Q-TOF) mass spectrometer (QSTAR Pulsar-i, AB Sciex) equipped with a nanospray ionization source. The protonated LIFAGK ion prepared by ESI was mass-selected and guided into the collision cell filled with Xe as the target gas at room temperature. The kinetic energy of the peptide ion E_{lab} varied from 30 to 50 eV in the laboratory frame. E_{lab} was the sum of the potential energy gained by the acceleration voltage and the kinetic energy of the peptide ion entering the collision cell in the absence of acceleration voltage. The relative collision energy in the center-of-mass frame E_{CM} was calculated using eq 8:

$$E_{CM} = \frac{m_{Xe}}{m_{\mathrm{ion}} + m_{Xe}} E_{lab}\,, \tag{8}$$

where m_{Xe} and m_{ion} denote the mass of Xe and the peptide ion, respectively.

To evaluate an increase in internal energy of the peptide ion by collisional excitation, we considered a soft-sphere model for collision between the peptide ion and Xe. In the collision cell at 298 K, the average speed of Xe (131.29 amu) was 219 m s^{-1}. Since the velocity of a singly protonated LIFAGK ion (647.81 amu) was 545.80 $\sqrt{E_{\mathrm{lab}}(eV)} \approx 3{,}000$–$3{,}900$ m s^{-1}, the peptide ion moved about 16 times faster than Xe. Therefore, a flying soft peptide ion encountered a slowly moving Xe atom and they formed a collision complex. Then, the Xe atom departed the peptide ion by following the laws of energy and momentum conservation. As a result, the relative collision energy E_{CM} imparted to the peptide ion was fully available to the internal excitation of the peptide ion. Thus, the internal energy of the activated peptide ion E_{int} can be written as follows:

$$E_{\mathrm{int}} = C_{\mathrm{vib}}(T_0) * T_0 + E_{CM} = C_{\mathrm{vib}}(T) * T\,, \tag{9}$$

where C_{vib} is the temperature-dependent vibrational heat capacity of the peptide ion, T_0 is the temperature of the peptide ion entering the collision cell, which was assumed to be 298 K, and T is the temperature of the activated peptide ion. Once T_0 and E_{CM} values are given, the temperature T can be determined using C_{vib}.

Calculations

To evaluate the vibrational heat capacity of a singly protonated LIFAGK ion, we calculated vibrational frequencies of five amino acids (L, I, F, A, G) and protonated lysine using a B3LYP level of the density functional theory with the 6-31G(d,p) basis set. We scaled vibrational frequencies by a factor of 0.9610.[13] Vibrational frequencies of the protonated peptide ion were estimated by excluding fifteen frequencies from six amino acids, i.e., three frequencies for each peptide bond. Both the O-H stretching [$\bar{\nu}$(O—H)] and the C-O-H bending [$\bar{\nu}$(C—O—H)] vibrations from five amino acids (L, I, F, A, G) were excluded and the N-H stretching vibration [$\bar{\nu}$(N—H)] from five amino acids (I, F, A, G, K) was excluded. Resulting vibrational frequencies are listed in Table 1.

The temperature-dependent vibrational heat capacity $C_{vib}(T)$ was calculated using eq 10:[14]

$$\frac{C_{\mathrm{vib}}(T)}{R} = \sum_i \frac{x_i^2 e^{x_i}}{\left(e^{x_i} - 1\right)^2};\ x_i = 1.44 \frac{\bar{\nu}_i\left(\mathrm{cm}^{-1}\right)}{T}\,, \tag{10}$$

where $\bar{\nu}_i$ is the vibrational frequency in units of cm^{-1}. There are 294 vibrational degrees of freedom in the protonated LIFAGK ion.

Table 1. Vibrational frequencies of protonated LIFAGK estimated using those of amino acids (L, I, F, A, G) and protonated lysine calculated at the B3LYP/6-31G(d,p) level. A scale factor of 0.9610 was used.[13]

amino acid	vibrational frequencies
Leu[a]	52, 61, 114, 149, 226, 230, 256, 280, 305, 330, 375, 424, 426, 517, 628, 710, 769, 794, 847, 871, 902, 908, 925, 937, 968, 1035, 1067, 1109, 1151, 1163, 1205, 1221, 1272, 1298, 1308, 1332, 1351, 1360, 1378, 1387, 1437, 1448, 1452, 1459, 1472, 1598, 1790, 2886, 2911, 2915, 2929, 2944, 2951, 2976, 2982, 2992, 3009, 3297, 3374, 3457
Ile[b]	55, 76, 97, 159, 208, 214, 248, 272, 292, 333, 345, 424, 472, 519, 636, 722, 754, 773, 821, 863, 868, 907, 942, 968, 1000, 1044, 1060, 1078, 1154, 1159, 1204, 1234, 1259, 1294, 1311, 1334, 1347, 1372, 1378, 1388, 1441, 1453, 1459, 1462, 1468, 1596, 1792, 2864, 2919, 2921, 2927, 2933, 2973, 2991, 2997, 2999, 3010, 3299, 3373, 3455
Phe[b]	26, 32, 74, 117, 190, 235, 277, 315, 343, 357, 402, 468, 507, 567, 611, 645, 686, 703, 740, 782, 797, 835, 857, 884, 899, 922, 943, 953, 975, 977, 1019, 1043, 1073, 1135, 1142, 1169, 1175, 1182, 1206, 1277, 1290, 1310, 1318, 1340, 1387, 1434, 1440, 1483, 1575, 1598, 1599, 1791, 2918, 2942, 2954, 3042, 3056, 3065, 3076, 3082, 3292, 3373, 3456
Ala[b]	73, 222, 265, 293, 344, 394, 510, 540, 705, 773, 832, 861, 908, 982, 1053, 1106, 1174, 1193, 1272, 1343, 1364, 1386, 1446, 1455, 1602, 1799, 2926, 2931, 2995, 3031, 3316, 3367, 3455
Gly[b]	89, 267, 312, 484, 527, 630, 796, 834, 867, 916, 1031, 1118, 1190, 1272, 1318, 1387, 1425, 1604, 1810, 2943, 2989, 3317, 3391, 3474
protonated Lys[c]	31, 43, 62, 91, 124, 157, 213, 223, 242, 269, 291, 334, 412, 441, 525, 624, 708, 724, 754, 788, 826, 844, 874, 889, 911, 944, 957, 980, 1017, 1055, 1076, 1105, 1167, 1202, 1203, 1248, 1262, 1288, 1294, 1302, 1312, 1332, 1361, 1370, 1388, 1444, 1449, 1455, 1456, 1470, 1603, 1603, 1608, 1778, 2905, 2908, 2923, 2927, 2947, 2950, 2981, 2990, 3042, 3267, 3274, 3357, 3360, 3386, 3467

[a] Both $\bar{\nu}$ (O—H) and $\bar{\nu}$ (C—O—H) were excluded; [b] $\bar{\nu}$ (O—H), $\bar{\nu}$ (C—O—H) and $\bar{\nu}$ (N—H) were excluded; [c] $\bar{\nu}$ (N—H) was excluded.

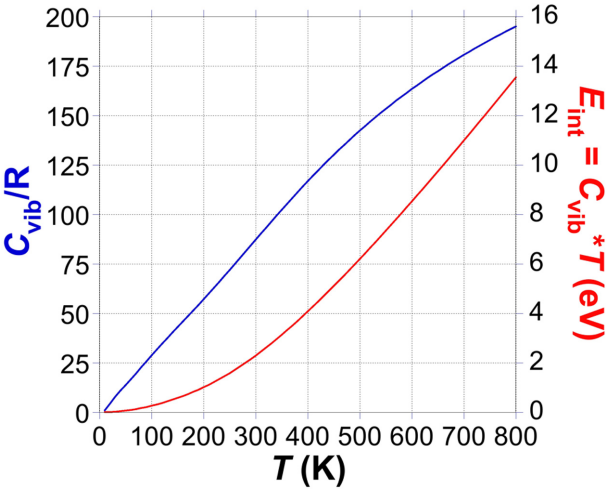

Figure 2. Vibrational heat capacity C_{vib} and internal energy of the protonated LIFAGK ion E_{int} as a function of temperature.

Results and Discussion

Both C_{vib} and E_{int} are plotted as a function of temperature in Figure 2. Unlike the classical vibrational heat capacity, the quantum mechanical C_{vib} gradually increases with temperature.

We compared the survival fraction of the protonated LIFAGK ion obtained from experiments[12] with that calculated using eq 7 as a function of collision energy. Since energy-variable CID experiments were carried out under a nearly single collision condition, where the mean-free-path of the peptide ion $\lambda = 1/\sigma[M]$ was made equal to the length of a collision cell l by adjusting the partial pressure of Xe [M], the product of k_1 and the transit time $\tau (= l/v)$ becomes one, independent of velocity v:[15]

$$k_1\tau = \sigma v[M]\frac{l}{v} = \sigma[M]l = \frac{l}{\lambda} = 1. \quad (11)$$

The survival fraction of the peptide ion at time t $(= 1/k_1)$ is thus:

$$\frac{[R]_\tau + [R^*]_\tau}{[R]_0} = \frac{[k_{PT}\tau e^{-1} - \exp(-k_{PT}\tau)]}{(k_{PT}\tau - 1)}. \quad (12)$$

In the case of $k_{PT}\tau >> 1$, where the proton transfer rate is much greater than the collision rate $(k_1 = \tau^{-1})$, the survival fraction reaches a limit of e^{-1}. On the other hand, in the case of $k_{PT}\tau << 1$, the survival fraction is close to one. Thus, the calculated survival fraction varies from one to e^{-1}. However, the experimental survival fraction changes from one to zero as the collision energy increases.[12] It has been found that the intensity of the total ion decreases fast with E_{lab}, indicating the discrimination against high mass and high velocity. To account for this instrument response function, we renormalized the survival fraction, as given in eq 13:

$$SF = \frac{1}{1-e^{-1}}\left\{\frac{\left[k_{PT}\tau e^{-1} - \exp(-k_{PT}\tau)\right]}{(k_{PT}\tau - 1)} - e^{-1}\right\}. \quad (13)$$

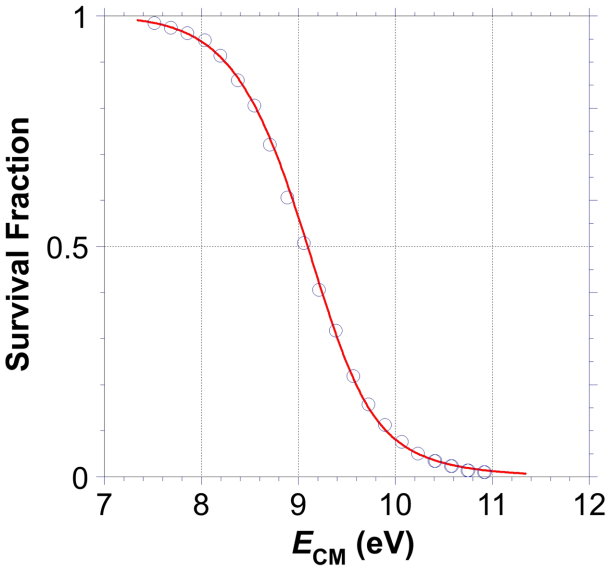

Figure 3. Survival fraction of the peptide ion as a function of collision energy in the center-of-mass frame E_{CM}. Open circle denotes experimental results taken from reference 12 and the solid line represents theoretical results obtained from eq 13.

Figure 3 shows the survival fraction obtained from experiments and theory. As E_{lab} increases from 30 to 50 eV, the transit time τ in the collision cell decreases from 3.87 to 5.00×10^{-5} s, as given in eq 14:

$$\tau = \frac{l}{v} = \frac{0.15 \text{ m}}{545.80\sqrt{E_{lab}(\text{eV})} \text{ m s}^{-1}} = 3.87 - 5.00 \times 10^{-5} \text{ s}. \quad (14)$$

Thus, the rate of collision k_1 varies in the range of 2.00–2.58×10^4 s^{-1}. Meanwhile, E_{int} increases from 7.52 to 10.92 eV and T increases from 591 to 693 K. This temperature range is close to the ion temperature of 615–635 K measured using a thermometer ion in N-acylated dipeptide tags.[16] The best-fit values for k_{PT} result in $k_{PT}\tau$ in the range of 0.25–42.5. Importantly, $\Delta G^{\dagger}$ shows the temperature dependence, as given in eq 15:

$$\Delta G^{\dagger} = \frac{\left(E_m + \Delta G^0\right)^2}{4E_m} = 1.78 - 1.15 \times 10^{-3} T \text{ (eV)}. \quad (15)$$

This temperature dependence of $\Delta G^{\dagger}$ implies that the slope of the parabolic potential energy curve in Figure 1 decreases with temperature. To estimate the Marcus reorganization energy E_m, we assumed that the free energy of the proton-transfer reaction ΔG^0 from R to I_N equals to the difference between the proton affinity (PA) of 10.32 eV for lysine[17] and the average PA of 9.54 eV for three adjacent backbone amide carbonyls of methyl esters of N-acetylated amino acids (F, A, G).[18] We also assumed that the entropy contribution to ΔG^0 is zero.[19,20] Using values of ΔG^0 = 0.78 eV and $\Delta G^{\dagger}$ = 1.44 eV at 298 K, we obtained 4.03 eV for E_m. If the temperature dependence of ΔG^0 is available, then it is possible to characterize the temperature dependence of the Marcus reorganization energy for the proton-transfer equilibria within the hydrogen-bonding environment in the protonated peptides.

Conclusions

We took an integrated thermochemical approach to describe the kinetics of energy-variable dissociation of a protonated lysine-terminated peptide ion. Temperature-dependent vibrational heat capacities were used to determine the temperature of the activated peptide ion under the assumption that the initial temperature of the intact peptide ion was 298 K and the relative collision energy was fully available to increase the internal energy of the peptide ion. The Marcus-theory-type rate equation for proton transfer was used to integrate a series of proton-transfer reactions that took place within the hydrogen-bond network in the peptide ion. Importantly, the best-fit curve showed that the free energy of the transition state slowly decreased with increasing collision energy.

Our thermochemical approach can be extended to parallel proton-transfer reactions including multiple N-protonated intermediates, enabling simulation of sequence-specific peptide fragmentation curves as a function of collision energy. For practical purpose, however, we need the temperatures of both the intact peptide ion and the activated peptide ion as well as the velocities of the peptide ion in the collision cell with/without acceleration voltage. Further studies are underway to apply our approach to the energy-variable dissociation of chemically modified peptides and other proton-bound host-guest complexes.

Acknowledgments

This work was supported by the National Research Foundation of Korea (NRF) grant funded by the Korea Government (MIST) (No. 2019R1A2C1006227).

References

1. Yoon, H.-J.; Seo, J.; Shin, S. K. *Mass Spectrom. Rev.* **2015**, 34, 209, DOI: 10.1002/mas.21435.
2. Wysocki, V.H.; Tsaprailis, G.; Smith, L. L.; Breci, L. A. *J. Mass Spectrom.* **2000**, 35, 1399, DOI: 10.1002/1096-9888(200012)35:12<1399::AID-JMS86>3.0.CO;2-R.
3. Paizs, B.; Lendvay, G.; Vécky, K.; Suhai, S. *Rapid Commun. Mass Spectrom.* **1999**, 13, 525, DOI: 10.1002/(SICI)1097-0231(19990330)13:6<525::AID-RCM519>3.0.CO;2-O.

4. Paizs, B.; Suhai, S. *Rapid Commun. Mass Spectrom.* **2002**, 16, 375, DOI: 10.1002/rcm.586.
5. Nelson, C. R.; Abutokaikah, M. T.; Harrison, A. G.; Bythell, B. J. *J. Am. Soc. Mass Spectrom.* **2016**, 27, 487, DOI: 10.1007/s13361-015-1298-4.
6. Csonka, I. P.; Paizs, B.; Lendvay, G.; Suhai, S. *Rapid Commun. Mass Spectrom.* **2000**, 14, 417, DOI: 10.1002/(SICI)1097-0231(20000331)14:6<417::AID-RCM885>3.0.CO;2-J.
7. Paizs, B.; Suhai, S. *Mass Spectrom. Rev.* **2005**, 24, 508, DOI: 10.1002/mas.20024.
8. Kim, H. W.; Rhee, Y. M.; Shin, S. K. *Phys. Chem. Chem. Phys.* **2018**, 20, 21068, DOI: 10.1039/C8CP03050B.
9. McLennan, D. J. *J. Chem. Ed.* **1976**, 53, 348.
10. Mayer, J. M. *J. Phys. Chem. Lett.* **2011**, 2, 1481, DOI: 10.1021/jz200021y.
11. Houston, P. L. Chemical Kinetics and Reaction Dynamics, International Edition, pp 155–159, McGraw Hill: Boston, **2001**.
12. Seo, J.; Yoon, H.-J.; Shin, S. K. *Int. J. Mass Spectrom.* **2019**, 435, 272. DOI: 10.1016/j.ijms.2018.11.001.
13. https://cccbdb.nist.gov/vibscalejust.asp, III.B.3.a. (XIII.C.1.) Precomputed vibrational scaling factors.
14. Benson, S. W. Thermochemical Kinetics, 2nd Edition, p. 42, John Wiley & Sons: New York, **1976**.
15. Varney, R. N. *Am. J. Phys.* **1971**, 39, 534, DOI: 10.1119/1.1986207.
16. Seo, J.; Suh, M. S.; Yoon, H.-J.; Shin, S. K. *J. Phys. Chem. B* **2012**, 116, 13982, DOI: 10.1021/jp308697v.
17. Hunter, E. P.; Lias, S. G. *J. Phys. Chem. Ref. Data* **1998**, 27, 413, DOI: 10.1063/1.556018.
18. Addario, V.; Guo, Y.; Chu, I. K.; Ling, Y.; Ruggerio, G.; Rodriquez, C.F.; Hopkinson, A.C.; Siu, K. W. M. *Int. J. Mass Spectrom.* **2002**, 219, 101, DOI: 10.1016/S1387-3806(02)00564-X.
19. Meot-Ner, M. *Chem. Rev.* **2012**, 112, PR22, DOI: 10.1021/cr200430n.
20. Harrison, A. G. *Mass Spectrom. Rev.* **1997**, 16, 201, DOI: 10.1002/(SICI)1098-2787(1997)16:4<201::AID-MAS3>3.0.CO;2-L.

